James R. Nagel

Electrostatic Simulation in 2D With the Boundary Element Method

©SHUTTERSTOCK.COM/PRETTYBOY80

A tutorial.

This article provides a detailed tutorial on the foundations of the boundary element method (BEM) by constructing a basic algorithm for 2D electrostatic systems. The geometry of a conductor is expressed as an N-sided polygon where each edge carries a surface charge density with linear continuity between nodes. The resulting basis functions are integrable using closed-form solutions, and the method of point matching yields a stable, invertible system matrix. We then expand the algorithm to include excitation by an impressed field as well as a simple method by which to model a floating conductor. The results are compared against analytic models, showing excellent precision with a relatively small amount of computational effort.

INTRODUCTION

There are many applications in physics and engineering where it is necessary to construct complex electrostatic models in two dimensions. For example, spread-spectrum time-domain reflectometry requires accurate transmission line models to locate electrical faults in aircraft wiring [1], [2]. The microstrip transmission line is a widespread embodiment used to construct complex microwave networks, but its properties are also difficult to model analytically [3], [4]. Electromagnetic transients in overhead power lines are a common problem requiring sophisticated multiconductor transmission line models [5]. Electrostatic film actuators use high-voltage charge separation to exert precision forces in soft robotics [6].

Due to the demand for such complex models, there is a persistent need for fast numerical techniques. One popular tool is the finite-difference method (FDM) [7], which works by converting the Poisson equation into a collection of finite-difference equations. The electric scalar potential is then sampled along a rectangular mesh within some region of interest and calculated at every grid point simultaneously.

Another popular tool is the finite-element method (FEM), which works very similarly to FDM by calculating the scalar potential throughout a region of interest [8], [9]. Rather than sampling the potential along a rectangular grid, however, the algorithm is free to place nodes arbitrarily in space. This allows FEM to represent curved geometries much more accurately as well as avoid oversampling nodes in less interesting regions of the model.

Despite its popularity and accuracy, FEM still suffers from a number of inherent mathematical difficulties. For example, a floating conductor is defined such that its net charge density is known, but not its electrical potential. Since it is not possible to impose an appropriate Dirichlet

Digital Object Identifier 10.1109/MAP.2022.3143440
Date of current version: 24 February 2022

Authorized licensed use limited to: UNIVERSITAT POLITECNICA DE CATALUNYA. Downloaded on December 16,2022 at 17:36:21 UTC from IEEE Xplore. Restrictions apply.

boundary condition, such a conductor is challenging to model without additional postprocessing steps [10], [11]. Another challenge for FEM is the absorbing boundary condition (or free-space boundary condition), which is difficult to implement for electrostatic fields without additionally complex procedures [12], [13]. Although one can alleviate this by simply placing the boundaries far away from the geometry of interest, doing so requires significant computational resources to sample the empty void.

As the name suggests, BEM operates by exploiting the fact that all surface charge density lies entirely along the edges of any conductive body in electrostatic equilibrium.

A third simulation method that avoids such limitations is the so-called BEM [14], which can be viewed as a special instance of the more generic method of moments (MoM) [15]. As the name suggests, BEM operates by exploiting the fact that all surface charge density lies entirely along the edges of any conductive body in electrostatic equilibrium. This completely removes the need to sample a mesh of empty space around the objects themselves, and the computational effort depends only on the complexity of the edges rather than the physical volume of interest. Free-space boundary conditions are then incorporated naturally by Green's functions and, thus, require no additional postprocessing to implement. The technique is even capable of directly modeling a floating conductor with almost no additional complexity to the algorithm.

Though BEM has many advantages, the choice of basis functions can introduce many challenges of its own. For example, the simplest basis is the delta function [16], which represents the system as a discrete collection of point charges (or line charges for the special case of 2D). Though easy to implement, the approximation tends to quickly break down for complex systems with high mesh density. The so-called self-terms in the system matrix also introduce problems of their own due to the inherent singularities that emerge from point-like charges.

For these reasons, it is much more common to utilize the pulse function as a basis rather than the delta. In this case, sources are treated as sectionally constant strips of uniform charge density, thereby removing the inherent singularity in the self-terms. The main tradeoff, however, is that this also introduces an undesirable complexity in the integration between the basis function and its kernel. Fortunately, the integral is still tractable for 2D systems, and so it still sees wide use in practical applications [5], [17], [18].

In this tutorial, the author derives a basic electrostatic simulation technique using BEM. The limitation to only two spatial dimensions serves as a useful starting point from which to simplify the subject for beginners while still maintaining value in a number of practical applications. The author further shows how to represent each source as a thin strip of linear surface charge density, thereby representing the sources under a triangular basis function rather than a pulse. The technique is widespread among BEM/MoM simulations, and it provides a significant boost to accuracy with a relatively minor increase in complexity. If this proves too difficult for a beginner, the technique can easily be reduced to a pulse-function basis by simply neglecting a few appropriate terms. The author then shows how to excite the system with an impressed field profile, followed by a new method for directly calculating the potential of floating conductors. Finally, the algorithm is validated against closed-form expressions to quantify both the speed and accuracy.

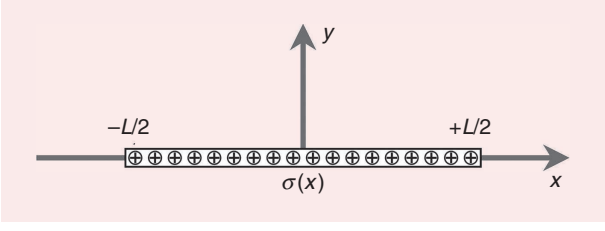

FIGURE 1. A thin strip of surface charge density is centered at the origin with length L. The surface charge density varies along the strip in accordance with the function $\sigma(x)$.

THIN STRIP OF LINEAR SURFACE CHARGE DENSITY

The foundation of BEM begins by imagining a thin strip of surface charge density having total length L. Depicted in Figure 1, the strip is centered at the origin and varies linearly in accordance with

$$\sigma(x) = \bar{\sigma} + \rho x \qquad (-L/2 \le x \le +L/2), \tag{1}$$

where $\bar{\sigma}$ is the mean surface charge density along the strip with units of C/m^2. The parameter ρ indicates a linear gradient from left to right and has units of (C/m^2)/m, or C/m^3.

Due to the presence of the surface charge, there naturally exists an electric scalar potential ϕ filling all space. To calculate ϕ, we begin by noting that an infinitesimally thin wire of constant linear charge density λ (C/m) satisfies

$$\phi(x, y) = -\frac{\lambda}{4\pi\epsilon_0} \ln\left|(x - x')^2 + (y - y')^2\right|, \tag{2}$$

where the coordinates (x, y) indicate the observation point, or test point, and the primed coordinates (x', y') indicate the location of the source wire. Note also that this expression

Authorized licensed use limited to: UNIVERSITAT POLITECNICA DE CATALUNYA. Downloaded on December 16,2022 at 17:36:21 UTC from IEEE Xplore. Restrictions apply.

implicitly assumes a ground reference at a distance of 1 m away from the source.

We next imagine a differential contribution $d\phi$ arising from some differential linear charge density $d\lambda$, written as

$$d\lambda(x') = \sigma(x')dx'. \tag{3}$$

Letting $y' = 0$, we integrate x' from $-L/2$ to $+L/2$ and arrive at

$$\phi(x,y) = \frac{-1}{4\pi\epsilon_0}\int_{-L/2}^{+L/2}(\bar{\sigma}+\rho x')\ln|(x-x')^2+y^2|\,dx'. \tag{4}$$

We thus have a Fredholm integral equation of the first kind, where $\sigma(x)$ is the basis function, and the natural log term represents the kernel.

Although somewhat imposing, the integral in (4) has a closed-form solution with no singularities. This makes it ideal when used as a basis function for numerical modeling. Begin by applying the substitution $u = x - x'$, which transforms (4) into

$$\phi(x,y) = -\left(\frac{\bar{\sigma}+\rho x}{4\pi\epsilon_0}\right)I_0(x,y) + \left(\frac{\rho}{4\pi\epsilon_0}\right)I_1(x,y), \tag{5}$$

where the integral functions I_0 and I_1 are defined as

$$I_0(x,y) = \int_{x-L/2}^{x+L/2}\ln|u^2+y^2|\,du, \quad \text{and} \tag{6}$$

$$I_1(x,y) = \int_{x-L/2}^{x+L/2}u\ln|u^2+y^2|\,du. \tag{7}$$

The exact solutions for these integrals have been noted as far back as 1984 by Wilton et al. [19], specifically for use in this sort of numerical application. For convenience, a thorough derivation is also provided in "Derivation of (6)" and "Derivation of (7)." We then separate the contributions from $\bar{\sigma}$ and ρ such that

$$\phi(x,y) = \bar{\sigma}f(x,y) + \rho g(x,y), \tag{8}$$

where the functions f and g satisfy

$$f(x,y) = -\frac{1}{4\pi\epsilon_0}I_0(x,y), \tag{9}$$

$$g(x,y) = -\frac{1}{4\pi\epsilon_0}[xI_0(x,y) - I_1(x,y)]. \tag{10}$$

Finally, the electric field intensity is calculated using $\mathbf{E} = -\nabla\phi$, and the partial derivatives are likewise provided in "Derivation of (6)" and "Derivation of (7)."

DERIVATION OF (6)

We are interested in evaluating the following integral function:

$$I_0(x,y) = \int_{x-L_h}^{x+L_h}\ln|u^2+y^2|\,du, \tag{6}$$

where $L_h = L/2$ is the half-length of the strip. Applying integration by parts, we can rewrite this expression as

$$I_0(x,y) = u\ln\left|u^2+y^2\right|\Big|_{x-L_h}^{x+L_h} - \int_{x-L_h}^{x+L_h}\frac{2u^2\,du}{u^2+y^2}. \tag{S1}$$

The second integral evaluates to

$$\int_{x-L_h}^{x+L_h}\frac{2u^2\,du}{u^2+y^2} = 2u - 2y\tan^{-1}\left(\frac{u}{y}\right)\Big|_{x-L_h}^{x+L_h}. \tag{S2}$$

Evaluating the limits of integration then yields

$$\begin{aligned} I_0(x,y) = &+(x+L_h)\ln\left|(x+L_h)^2+y^2\right| \\ &-(x-L_h)\ln\left|(x-L_h)^2+y^2\right| \\ &+2y\tan^{-1}\left(\frac{x+L_h}{y}\right) \\ &-2y\tan^{-1}\left(\frac{x-L_h}{y}\right) \\ &-4L_h. \end{aligned} \tag{S3}$$

At first glance, (S3) appears to have possible singularities, but they all vanish upon closer inspection. For example, when $y = 0$, the terms with inverse tangents both evaluate to zero. Likewise, the logarithms appear to have singularities at $(x, y) = (\pm L_h, 0)$, but both terms evaluate to zero as well.

It is constructive to rewrite (S3) using polar notation. Begin by defining the radial distances r_1 and r_2 such that

$$r_1^2 = (x+L_h)^2 + y^2, \quad \text{and} \tag{S4}$$

$$r_2^2 = (x-L_h)^2 + y^2, \tag{S5}$$

which represent distances from each endpoint of the strip to a test point at (x, y). Likewise, we may define the angles θ_1 and θ_2 such that

$$\theta_1 = \tan^{-1}\left(\frac{x+L_h}{y}\right), \quad \text{and} \tag{S6}$$

$$\theta_2 = \tan^{-1}\left(\frac{x-L_h}{y}\right), \tag{S7}$$

which indicate the angles between each endpoint of the strip and test point. The function I_0 thus simplifies to

$$\begin{aligned} I_0(x,y) = &(x+L_h)\ln|r_1^2| - (x-L_h)\ln|r_2^2| \\ &+2y(\theta_1-\theta_2) - 4L_h. \end{aligned} \tag{S8}$$

We would also like to know the gradient of I_0, which necessitates the evaluation of $\partial I_0/\partial x$ and $\partial I_0/\partial y$. These calculations are fairly straightforward, resulting in

$$\frac{\partial I_0}{\partial x} = \ln\left(\frac{r_1^2}{r_2^2}\right), \tag{S9}$$

$$\frac{\partial I_0}{\partial y} = 2(\theta_1-\theta_2). \tag{S10}$$

Authorized licensed use limited to: UNIVERSITAT POLITECNICA DE CATALUNYA. Downloaded on December 16,2022 at 17:36:21 UTC from IEEE Xplore. Restrictions apply.

As a demonstration, Figure 2 shows the resulting scalar potential and electric field profile for a thin strip with length $L = 10$ mm. The linear charge density was given a value of $\sigma(-L/2) = -1\ \text{nC/m}^2$ for the left tip and $\sigma(+L/2) = +1\ \text{nC/m}^2$ for the right tip. Thus, the mean surface charge density is $\bar{\sigma} = 0$ with a linear slope of $\rho = 200\ \text{nC/m}^2/\text{m}$.

DERIVATION OF (7)

We are next interested in evaluating

$$I_1(x, y) = \int_{x-L_h}^{x+L_h} u \ln|u^2 + y^2|\, du. \tag{7}$$

Integration, in this case, is fairly straightforward, resulting in

$$I_1 = \left(\frac{r_1^2}{2}\right)(\ln|r_1^2| - 1) - \left(\frac{r_2^2}{2}\right)(\ln|r_2^2| - 1). \tag{S11}$$

Th evaluation of the partial derivatives on I_1 then leads to

$$\frac{\partial I_1}{\partial x} = (x + L_h)\ln(r_1^2) - (x - L)\ln(r_2^2), \tag{S12}$$

$$\frac{\partial I_1}{\partial y} = y \ln\left(\frac{r_1^2}{r_2^2}\right). \tag{S13}$$

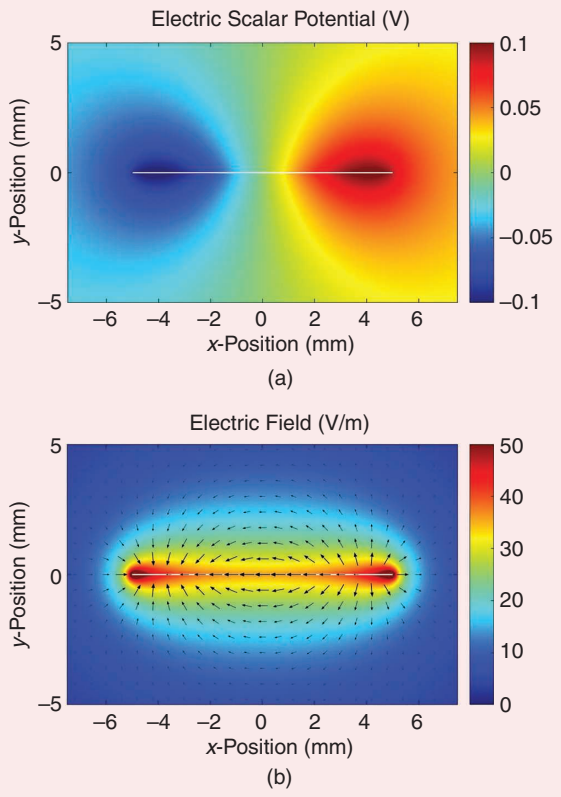

FIGURE 2. (a) The electric scalar potential ϕ arising from a thin strip of charge density with length $L = 10$ mm. The surface charge density varies linearly from left to right, starting with $\sigma = -1\ \text{nC/m}^2$ at the left tip and ending with $+1\ \text{nC/m}^2$ at the right tip. (b) The corresponding electric field **E** from the same strip.

COORDINATE TRANSFORMATIONS

For generality, it is necessary to consider a similar strip of charge density that has been offset and rotated in space. Depicted in Figure 3, the center of the strip is positioned at (x_0, y_0), followed by a rotation angle of φ. To calculate ϕ, we must transform to the new coordinate system (u, v) according to

$$u(x, y) = +(x - x_0)\cos\varphi + (y - y_0)\sin\varphi, \tag{11}$$

$$v(x, y) = -(x - x_0)\sin\varphi + (y - y_0)\cos\varphi. \tag{12}$$

The electric scalar potential for the transformed strip still follows (5) but with the coordinates (x, y) replaced with (u, v). Letting $u = u(x, y)$ and $v = v(x, y)$, the solution may be written as

$$\phi(x, y) = \bar{\sigma} f(u, v) + \rho g(u, v). \tag{13}$$

To obtain the electric field intensity **E** of a rotated strip, we apply a similar transformation to the x and y components. However, this will result in an electric field with basis vectors along u and v. To convert back into the (x, y) basis, it is necessary to transform the electric field components using

$$E_x = E_u \cos(\varphi) - E_v \sin(\varphi), \tag{14}$$

$$E_y = E_u \sin(\varphi) + E_v \cos(\varphi). \tag{15}$$

LINEAR INVERSION

An important implication of (13) is the capacity to calculate $\bar{\sigma}$ and ρ when given two samples of ϕ from the space nearby. To illustrate, suppose we are given the two potentials ϕ_1 and ϕ_2 at the test locations (x_1, y_1) and (x_2, y_2). The result is a linear system of equations with the form

$$\phi_1 = \bar{\sigma} f(x_1, y_1) + \rho g(x_1, y_1), \tag{16}$$

$$\phi_2 = \bar{\sigma} f(x_2, y_2) + \rho g(x_2, y_2). \tag{17}$$

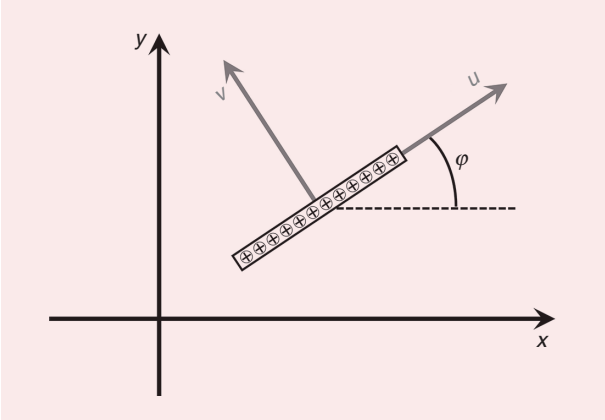

FIGURE 3. A thin strip of charge density offset and rotated to the (u, v) coordinate system.

Authorized licensed use limited to: UNIVERSITAT POLITECNICA DE CATALUNYA. Downloaded on December 16,2022 at 17:36:21 UTC from IEEE Xplore. Restrictions apply.

Thus, a simple inversion of the system will return the original values of $\bar{\sigma}$ and ρ.

When looking closely at the image of scalar potential in Figure 2, it is important to notice that ϕ cannot be sampled arbitrarily. In particular, there is a symmetry about the x-axis, which means any pair of test points with the form $(x, \pm y)$ is ill posed. This is because the kernel functions f and g return the same value at both locations, and the system of equations becomes singular. It is, therefore, important to be mindful of how the test samples are chosen so as to maintain a stable solution.

If the complexity of triangular basis functions is too much for a beginner, then this formalism readily simplifies with the use of pulse functions.

In the language of BEM/MoM simulation, this basic inversion technique is known as *point matching*, or *collocation*. In practice, however, there exists a wide variety of methods by which one could recover $\bar{\sigma}$ and ρ. For example, we could attempt to overdetermine the system by sampling ϕ along three test locations rather than two. The solution could then recover any values of $\bar{\sigma}$ and ρ that minimize the total squared error along all three points simultaneously. Other techniques may try to minimize the error across a continuous interval, while others still may even place different weights on the various errors [20]. Such techniques are common when simulating complex scattering models but generally not necessary for basic electrostatics.

CONNECTED POLYGONS

Let us now consider a connected polygon like the one depicted in Figure 4. The polygon consists of N connected strips of surface charge density with a linear variation between nodes. Each strip, or edge, has a mean charge density $\bar{\sigma}_n$, a slope ρ_n, a total length L_n, and a rotation angle φ_n. We further define ϕ_{mn} as the scalar potential at test point (x_m, y_m) arising from the nth edge of the polygon. This implies

$$\phi_{mn} = \bar{\sigma}_n f_n(x_m, y_m) + \rho_n g_n(x_m, y_m), \tag{18}$$

where f_n and g_n represent the corresponding kernels from the same edge. The total scalar potential $\phi(x_m, y_m)$ arising from the entire polygon is then defined as a linear superposition over each individual contribution, meaning that

$$\phi(x_m, y_m) = \sum_{n=1}^{N} \phi_{mn}. \tag{19}$$

The implication of (19) is that, if we are given the value of ϕ at 2 N different test points, then we may recover the full array of $\bar{\sigma}_n$ and ρ_n values along the polygon. In practice, however, the requirement of continuity between nodes allows us to reduce the total number of required samples down to N. To see how, we first define σ_n as the surface charge density at node n of the polygon. Each edge of the polygon may then be defined by a start node at n and a stop node at $n+1$. (Note that the ordering of the nodes is important, as it allows us to keep track of the outward unit normal to the polygon.) The values of $\bar{\sigma}_n$ and ρ_n corresponding to the nth edge thus satisfy

$$\bar{\sigma}_n = \frac{(\sigma_n + \sigma_{n+1})}{2}, \tag{20}$$

$$\rho_n = \frac{(\sigma_{n+1} - \sigma_n)}{L_n}, \tag{21}$$

where the special case of $n+1 = N+1$ wraps around back to $n+1 \to 1$. The total scalar potential $\phi_m = \phi(x_m, y_m)$ arising from the entire polygon can now be written as

$$\phi_m = \sum_{n=1}^{N} \left(\frac{\sigma_n + \sigma_{n+1}}{2}\right) f_{mn} + \left(\frac{\sigma_{n+1} - \sigma_n}{L_n}\right) g_{mn}, \tag{22}$$

where $f_{mn} = f_n(x_m, y_m)$ and $g_{mn} = g_n(x_m, y_m)$.

Expressions like (22) are far easier to manipulate if written with matrix–vector notation. We begin by defining the column vector $\mathbf{x}$ of unknown charge density nodes such that

$$\mathbf{x} = [\sigma_1, \sigma_2, \ldots, \sigma_N]^T. \tag{23}$$

We may further define the forcing vector $\mathbf{b}$ to indicate a collection of scalar potentials along N corresponding test locations:

$$\mathbf{b} = [\phi_1, \phi_2, \ldots, \phi_N]^T. \tag{24}$$

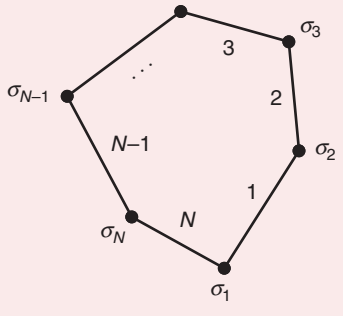

FIGURE 4. A connected polygon of N surface charge densities with linear continuity between nodes. Each node has a surface charge density σ_n that connects the edges.

Authorized licensed use limited to: UNIVERSITAT POLITECNICA DE CATALUNYA. Downloaded on December 16,2022 at 17:36:21 UTC from IEEE Xplore. Restrictions apply.

The kernel matrices $\mathbf{F}$ and $\mathbf{G}$ are then defined such that

$$F_{mn} = f(u_n(x_m, y_m), v_n(x_m, y_m)), \tag{25}$$

$$G_{mn} = g(u_n(x_m, y_m), v_n(x_m, y_m)). \tag{26}$$

To capture the mean and slope terms before f_{mn} and g_{mn}, respectively, it helps to define the averaging matrix $\mathbf{A}$ such that

$$\mathbf{A} = \frac{1}{2}\begin{bmatrix} 1 & 1 & 0 & 0 & \cdots & 0 & 0 \\ 0 & 1 & 1 & 0 & \cdots & 0 & 0 \\ & \vdots & & & \ddots & \vdots & \\ 0 & 0 & 0 & 0 & \cdots & 1 & 1 \\ 1 & 0 & 0 & 0 & \cdots & 0 & 1 \end{bmatrix}. \tag{27}$$

We further define the slope matrix $\mathbf{S}$ using

$$\mathbf{S} = \begin{bmatrix} -1/L_1 & +1/L_1 & 0 & \cdots & 0 \\ 0 & -1/L_2 & +1/L_2 & \cdots & 0 \\ & \vdots & & \ddots & \vdots \\ +1/L_N & 0 & 0 & \cdots & -1/L_N \end{bmatrix}. \tag{28}$$

Putting it all together, the system of equations represented by (22) is converted into a compact matrix–vector equation with the form

$$\mathbf{b} = (\mathbf{FA} + \mathbf{GS})\mathbf{x}. \tag{29}$$

We now define the system matrix as $\mathbf{M} = \mathbf{FA} + \mathbf{GS}$, and the solution for $\mathbf{x}$ becomes

$$\mathbf{x} = \mathbf{M}^{-1}\mathbf{b}. \tag{30}$$

It is worth noting that the choice of test points is completely arbitrary so long as the corresponding scalar potentials ϕ_m are known. For perfect electrical conductors (PECs), the obvious choice is within the PEC itself since all values are presumably known and constant. Matrix conditioning is the only limiting factor, so it is important to spread out the test points as much as possible. In practice, the nodes of the polygon itself seem to work very well at maintaining stability.

If the complexity of triangular basis functions is too much for a beginner, then this formalism readily simplifies with the use of pulse functions. All one needs to do is replace the system matrix with $\mathbf{M} = \mathbf{F}$ and then choose test points along the center of each polygon edge. The vector $\mathbf{x}$ is then reinterpreted as an array containing only the mean charge densities $\bar{\sigma}_n$, and the solution follows accordingly from (30).

MULTIPLE POLYGONS

In practice, a single polygon of constant potential is not very interesting, but an arbitrary collection of K such polygons can be used to model a wide variety of useful systems. To that end, it is helpful to define a notation that seamlessly coordinates the interaction of several polygons at once. We begin by defining the charge density σ_n^k to represent the nth node of the kth polygon. The kth polygon is then associated with a row vector $\mathbf{x}_k$ of unknown charge density samples, such that

$$\mathbf{x}_k = [\sigma_1^k, \sigma_2^k, \ldots, \sigma_{N_k}^k], \tag{31}$$

where N_k is the total number of nodes on the kth polygon. We then define the global unknown vector $\mathbf{x}$ (a column vector) as a concatenation of each unknown vector across all polygons:

$$\mathbf{x} = [\mathbf{x}_1, \mathbf{x}_2, \ldots, \mathbf{x}_K]^T. \tag{32}$$

We may further associate the kth polygon with an array of test potentials $\mathbf{b}_k$, written as

$$\mathbf{b}_k = [\phi_k, \phi_k, \ldots, \phi_k]^T, \tag{33}$$

where ϕ_k is the uniform scalar potential of the same polygon. Similar to (32), there also exists a corresponding global forcing vector $\mathbf{b}$.

Under this notation, the ℓth potential array $\mathbf{b}_\ell$ is generated by adding up the contributions due to individual sources across all polygons in the system. Using matrix–vector summation, we may write this as

$$\mathbf{b}_\ell = \sum_{k=1}^{K} (\mathbf{F}_{\ell k}\mathbf{A}_k + \mathbf{G}_{\ell k}\mathbf{S}_k)\mathbf{x}_k. \tag{34}$$

In this context, $\mathbf{A}_k$ and $\mathbf{S}_k$ are square matrices with size $N_k \times N_k$ representing the average and slope matrix for the kth polygon. The kernel matrices $\mathbf{F}_{ik}$ and $\mathbf{G}_{ik}$ likewise match the potentials on the ith polygon due to charges on the kth. We further define the global system matrix $\mathbf{M}$ as a $K \times K$ block matrix satisfying

$$\mathbf{M} = \begin{bmatrix} \mathbf{M}_{11} & \mathbf{M}_{12} & \cdots & \mathbf{M}_{1K} \\ \mathbf{M}_{21} & \mathbf{M}_{22} & \cdots & \mathbf{M}_{2K} \\ \vdots & \vdots & \ddots & \vdots \\ \mathbf{M}_{K1} & \mathbf{M}_{K2} & \cdots & \mathbf{M}_{KK} \end{bmatrix}, \tag{35}$$

where $\mathbf{M}_{\ell k} = \mathbf{F}_{\ell k}\mathbf{A}_k + \mathbf{G}_{\ell k}\mathbf{S}_k$. The global matrix–vector equation now satisfies the original $\mathbf{Mx} = \mathbf{b}$ and is, again, solved using (30).

IMPRESSED FIELDS

A useful advantage of BEM is the capacity to directly excite a system with an impressed electric field $\mathbf{E}_0$. In principle, any arbitrary field profile may be inserted, but the uniform field profile is a simple example with many useful applications. Therefore, we express $\mathbf{E}_0$ as

$$\mathbf{E}_0 = E_{x0}\hat{\mathbf{x}} + E_{y0}\hat{\mathbf{y}}. \tag{36}$$

Authorized licensed use limited to: UNIVERSITAT POLITECNICA DE CATALUNYA. Downloaded on December 16,2022 at 17:36:21 UTC from IEEE Xplore. Restrictions apply.

Using the origin as a point of reference, such a field implies an impressed scalar potential ϕ_0 with the form

$$\phi_0(x, y) = -E_{x0}x - E_{y0}y. \quad (37)$$

Next, we decompose the total scalar potential ϕ_{tot} as a superposition between the impressed potential, which is arbitrary, and induced potential, which arises from the surface charge densities scattered throughout the simulation domain. For a PEC, however, the total potential on the kth polygon is simply a constant $\phi_{\text{tot}} = \phi_k$. The induced potential ϕ_m^k at the mth test point along polygon k is thus written as

$$\phi_m^k = \phi_k - \phi_0(x_m, y_m). \quad (38)$$

Using (33), the individual forcing vector for the kth polygon now takes on the form of

$$\mathbf{b}_k = \phi_k - \mathbf{b}_0, \quad (39)$$

where each element in $\mathbf{b}_0$ represents the impressed potential ϕ_0 at its corresponding test point.

FLOATING CONDUCTORS

Another desirable feature of any electrostatic simulation algorithm is the floating conductor—i.e., a conductive body with some net linear charge density λ_ℓ but whose static potential ϕ_ℓ is unknown. In this situation, the scalar potential ϕ_ℓ becomes a new variable in the linear system of equations. Thus, to guarantee a unique solution, we require an extra equation that expresses the desired condition.

Consider the ℓth polygon with mean surface charge density $\bar{\sigma}_n^\ell$ along the nth edge. The total linear charge density λ_ℓ across the entire polygon may then be calculated as

$$\sum_{n=1}^{N_\ell} L_n^\ell \bar{\sigma}_n^\ell = \lambda_\ell, \quad (40)$$

where L_n^ℓ indicates the length of the nth edge on the ℓth polygon. In terms of the charge density samples along each individual node, this expression simplifies into

$$\frac{1}{2}\sum_{n=1}^{N_\ell} L_n^\ell(\sigma_n^\ell + \sigma_{n+1}^\ell) = \lambda_\ell, \quad (41)$$

Where, again, the special case of $n + 1 = N_\ell$ is replaced with $n + 1 \to 1$.

Another desirable feature of any electrostatic simulation algorithm is the floating conductor—i.e., a conductive body with some net linear charge density λ_ℓ but whose static potential ϕ_ℓ is unknown.

The incorporation of this new condition into the system matrix seems challenging, but there is a straightforward procedure we can utilize. It works by introducing an intermediate processing step that calculates the potential of all floating polygons before constructing the forcing vector $\mathbf{b}$. We begin by defining the unit pulse vector $\mathbf{u}_k$ as a vector containing all zeros except for those indexes corresponding to nodes on the kth polygon. If we then fill these indexes with all ones, the global forcing vector $\mathbf{b}$ can be rewritten as

$$\mathbf{b} = -\mathbf{b}_0 + \sum_{k=1}^{K} \mathbf{u}_k \phi_k, \quad (42)$$

where, again, $\mathbf{b}_0$ indicates the impressed potential due to outside forces.

For a system of PECs with known scalar potential across all polygons, each value of ϕ_k may be treated as a given, and (42) reduces identically to (33). If, however, some of the ϕ_k are unknown, then we need to calculate them before constructing the forcing vector $\mathbf{b}$. To that end, we substitute (42) into (29) to find

$$\mathbf{M}\mathbf{x} = -\mathbf{b}_0 + \sum_{k=1}^{K} \mathbf{u}_k \phi_k. \quad (43)$$

We next multiply both sides by the inverse system matrix $\mathbf{M}^{-1}$ to find

$$\mathbf{x} = -\mathbf{M}^{-1}\mathbf{b}_0 + \sum_{k=1}^{K} \mathbf{M}^{-1}\mathbf{u}_k \phi_k. \quad (44)$$

Finally, we need to impose the condition expressed by (41), whereby the net linear charge density on conductor ℓ is equal to λ_ℓ. For this step, we introduce the edge-length vector $\mathbf{e}_\ell$, whereby

$$\mathbf{e}_\ell^T \mathbf{x} = \lambda_\ell. \quad (45)$$

As with the unit step vector, all elements in $\mathbf{e}_\ell$ are zero except for those corresponding to nodes on the ℓth polygon. In that case, the nth nonzero entry satisfies

$$e_{\ell,n} = \frac{L_n^\ell + L_{n+1}^\ell}{2}, \quad (46)$$

where, yet again, the special case of $n + 1 = N_\ell + 1$ is replaced with $n + 1 = 1$.

If we next multiply both sides of (44) by $\mathbf{e}_\ell^T$, we find that

$$\lambda_\ell + \mathbf{e}_\ell^T \mathbf{M}^{-1}\mathbf{b}_0 = \sum_{k=1}^{K} (\mathbf{e}_\ell^T \mathbf{M}^{-1}\mathbf{u}_k)\phi_k. \quad (47)$$

Authorized licensed use limited to: UNIVERSITAT POLITECNICA DE CATALUNYA. Downloaded on December 16,2022 at 17:36:21 UTC from IEEE Xplore. Restrictions apply.

When repeated over all K polygons (or even just the floating polygons), the result is a $K \times K$ matrix–vector equation in terms of the system matrix $\mathbf{M}$ and impressed field vector $\mathbf{b}_0$. This allows us to directly calculate all unknown potentials ϕ_k arising from any floating conductors. These new potentials are then inserted into the final forcing vector $\mathbf{b}$ through (42), and the system is solved normally via (30).

It is interesting to note that this intermediate processing step adds relatively little computational complexity to the simulation. In practice, the most computationally intensive step in an algorithm like this is the construction and inversion of the system matrix $\mathbf{M}$. However, this step was already necessary to solve (30), which means each term in (47) is comparatively fast to calculate after the fact.

The agreement between the simulated field profile and its exact solution is remarkable, and a side-by-side comparison reveals little perceptible difference.

VALIDATION

To validate the performance of BEM, we perform a benchmark against a known analytic model. One classic system is the two-wire transmission line depicted in Figure 5. Each wire has a radius a with equal but opposite scalar potential $\pm V_0$. The left wire is positioned at the origin, while the right wire is centered at $x = d$. The solution for the scalar potential is outlined in [21], and the characteristic capacitance between wires satisfies

$$C' = \frac{\pi \epsilon_0}{\cosh^{-1}\left(\frac{d}{2a}\right)}. \tag{48}$$

Figure 6 shows a side-by-side comparison of the electric field profile $|\mathbf{E}|$ using both closed-form (exact) calculations and a BEM simulation. The simulated wires were constructed using two circular polygons with 45 angular samples each ($N = 90$ nodes in total). Each circle was given a radius of $a = 1$ m, separation distance of $d = 2.5$ m, and scalar potential ± 1 V (positive on the left and negative on the right). After running the simulation under MATLAB on a standard laptop computer, the time required to construct and invert the system matrix required roughly 10–15 ms. For those interested in performing a benchmark themselves, the original source code is freely available on Code Ocean [22].

The agreement between the simulated field profile and its exact solution is remarkable, and a side-by-side comparison reveals little perceptible difference. Figure 6, therefore, also shows the absolute error magnitude at each location in the field profile. The greatest error appears to concentrate around the edges of the polygon, where flat surfaces are unable to perfectly follow the curved arc of a circle. However, once we move a short distance away from the surface, the error rapidly drops to a scale of 0.5% or less.

To calculate the characteristic capacitance between wires, we simply apply (40) to the left wire and then calculate the total linear charge density λ. The characteristic capacitance then follows from the definition $C' = \lambda / \Delta V$. To validate the convergence of BEM, C' was calculated as a function of angular samples in each

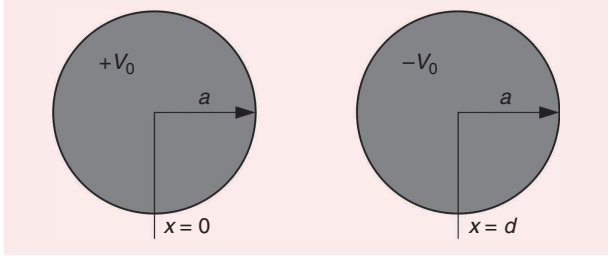

FIGURE 5. Two metal wires with radius a are separated by distance d. The cylinders are charged with equal and opposite potential V_0.

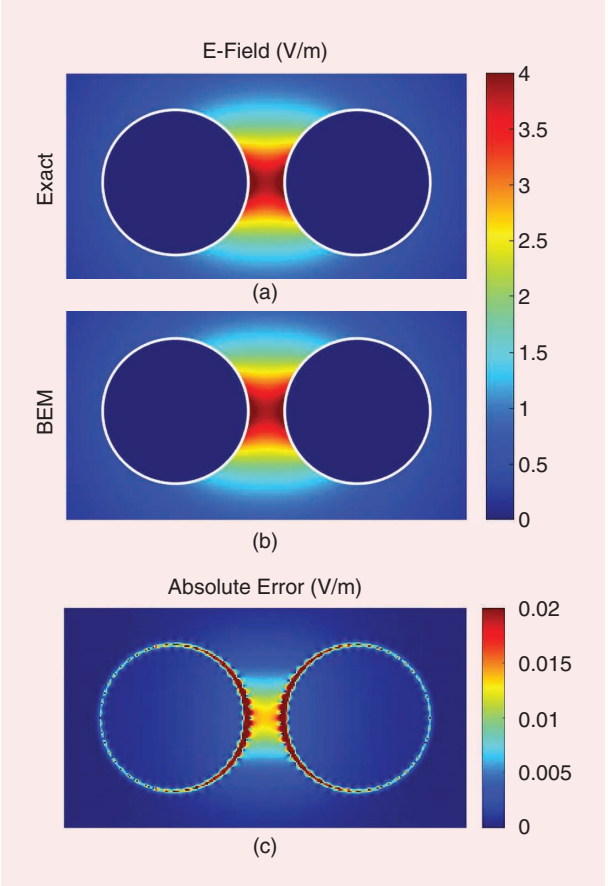

FIGURE 6. (a) The exact field profile compared against (b) a numerical simulation. Each wire has a radius of $a = 1$ m with a separation distance of $d = 2.5$ m and potential of ± 1 V. (The white outlines were added for clarity.) (c) The absolute error between the two.

Authorized licensed use limited to: UNIVERSITAT POLITECNICA DE CATALUNYA. Downloaded on December 16,2022 at 17:36:21 UTC from IEEE Xplore. Restrictions apply.

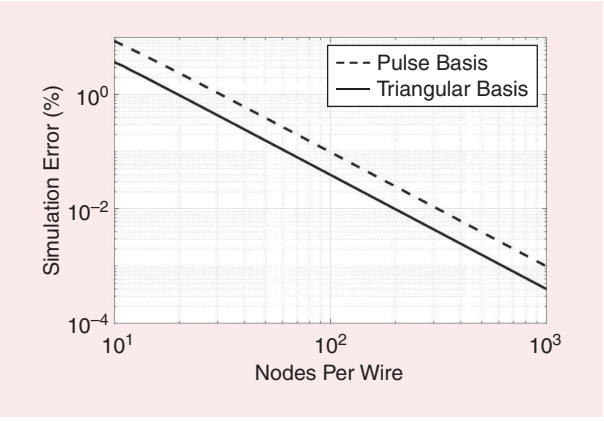

FIGURE 7. The percent error between the simulated characteristic capacitance C' and its exact value.

wire. The percent error was then calculated against its true value of $C' = 40.1304$ pC/m and is plotted in Figure 7.

As expected, the simulated capacitance converges smoothly to the correct value as angular resolution increases. For comparison, the same simulation was also performed using pulse basis functions. The results show that the use of triangular basis functions reduced the error to roughly 40% that of the pulse functions.

DISCUSSION

BEM is a powerful simulation technique that rapidly calculates the surface charge density along a collection of polygons with fixed potentials. Unlike FEM, which must sample a void of empty space around the region of interest, the computational complexity of BEM depends only on the complexity of the edges (hence, the term *boundary elements*). The method naturally incorporates a free-space boundary condition beyond the polygons, and it can even model floating conductors with relative ease.

For the sake of simplicity, this tutorial has shown only how to model the behavior of PECs in electrostatic equilibrium. Ideally, we would like to further incorporate the presence of dielectric bodies, and the basic procedure has already been demonstrated in three dimensions using pulse basis functions [23], [24]. There is also value in applying similar methods to magnetostatic simulation, and the mathematical formalism in 2D is virtually identical to that of the electrostatic case [7]. Another widespread application is electromagnetic scattering, for which BEM is, likewise, well suited [20]. All that would change is the choice of kernel function and testing procedure, but the basic inversion technique is essentially the same.

Despite the numerous advantages of BEM, there are still certain situations that can destabilize the results. In particular, sharp corners are especially problematic due to the infinite charge density that accumulates at the tips. Fortunately, a number of different techniques can mitigate this effect [25].

AUTHOR INFORMATION

James R. Nagel (james.nagel@utah.edu) is with the Department of Electrical and Computer Engineering, University of Utah, Salt Lake City, Utah, 84112, USA.

REFERENCES

[1] L. A. Griffiths, R. Parakh, C. Furse, and B. Baker, "The invisible fray: A critical analysis of the use of reflectometry for fray location," *IEEE Sensors J.*, vol. 6, no. 3, pp. 697–706, Jun. 2006, doi: 10.1109/JSEN.2006.874017.

[2] E. J. Lundquist, J. R. Nagel, S. Wu, B. Jones, and C. Furse, "Advanced forward methods for complex wire fault modeling," *IEEE Sensors J.*, vol. 13, no. 4, pp. 1172–1179, Apr. 2013, doi: 10.1109/JSEN.2012.2227996.

[3] I. J. Bahl and D. K. Trivedi, "A designer's guide to microstrip line," *Microwaves*, vol. 16, no. 5, pp. 174–182, 1977.

[4] L. G. Maloratsky, "Reviewing the basics of microstrip lines," *Microw. RF*, vol. 39, no. 3, pp. 79–88, 2000.

[5] M. Shafieipour, Z. Chen, A. Menshow, J. D. Silva, and V. Okhmatovski, "Efficiently computing the electrical parameters of cables with arbitrary cross-sections using the method-of-moments," *Electric Power Syst. Res.*, vol. 162, pp. 37–49, Sep. 2018, doi: 10.1016/j.epsr.2018.04.013.

[6] W. Wang, D. Fan, R. Zhu, P. Wang, Y. Zhao, and H. Wang, "Modeling and optimization of electrostatic film actuators based on the method of moments," *Soft Robot.*, vol. 8, no. 6, pp. 651–661, Dec. 2021, doi: 10.1089/soro.2020.0099.

[7] J. R. Nagel, "Numerical solutions to Poisson equations using the finite-difference method [Education Column]," *IEEE Antennas Propag. Mag.*, vol. 56, no. 4, pp. 209–224, Aug. 2014, doi: 10.1109/MAP.2014.6931698.

[8] A. C. Polycarpou, *Introduction to the Finite Element Method in Electromagnetics*. San Rafael, CA, USA: Morgan & Claypool, 2006.

[9] J.-M. Jin, *The Finite Element Method in Electromagnetics*, 3rd ed. Hoboken, NJ, USA: Wiley, 2014.

[10] D. Deleruyelle and G. Micolau, "On the electrostatic behavior of floating nanoconductors," *Solid-State Electron.*, vol. 52, no. 1, pp. 17–24, 2008, doi: 10.1016/j.sse.2007.07.008.

[11] D. J. Rincon, E. Aguilera, and J. C. Chacon, "Numerical treatment of floating conductors based on the traditional finite element formulation," *IEEE Trans. Microw. Theory Techn.*, vol. 32, no. 11, pp. 1441–1448, Nov. 1984.

[12] G. K. Gothard, S. M. Rao, T. K. Sarkar, and M. S. Palma, "Finite element solution of open region electrostatic problems incorporating the measured equation of invariance," *IEEE Microw. Guided Wave Lett.* (1991–2000)*, vol. 5, no. 8, pp. 252–254, Aug. 1995, doi: 10.1109/75.401076.

[13] D. C. Meeker, "Improvised asymptotic boundary conditions for electrostatic finite elements," *IEEE Trans. Magn.*, vol. 50, no. 6, Jun. 2014, Art no. 7,400,609, doi: 10.1109/TMAG.2014.2300196.

[14] J. T. Katsikadelis, *Boundary Elements: Theory and Practice*. Oxford, U.K.: Elsevier, 2002.

[15] W. C. Gibson, *The Method of Moments in Electromagnetics*, 2nd ed. Boca Raton, FL, USA: CRC Press, 2015.

[16] L. L. Tsai and C. E. Smith, "Moment methods in electromagnetics for undergraduates," *IEEE Trans. Educ.*, vol. 21, no. 1, pp. 14–22, Feb. 1978, doi: 10.1109/TE.1978.4321178.

[17] C. E. Smith and R.-S. Chang, "Microstrip transmission line with finite-width dielectric," *IEEE Trans. Microw. Theory Techn.*, vol. 28, no. 2, pp. 90–94, Feb. 1980, doi: 10.1109/TMTT.1980.1130015.

[18] C. A. Balanis, *Advanced Engineering Electromagnetics*, 2nd ed. Hoboken, NJ, USA: Wiley, 2012.

[19] D. R. Wilton, S. M. Rao, A. W. Glisson, O. M. Al-Bundak, and C. M. Butler, "Potential integrals for uniform and linear source distributions on polygonal and polyhedral domains," *IEEE Trans. Antennas Propag.*, vol. 32, no. 3, pp. 276–281, Mar. 1984, doi: 10.1109/TAP.1984.1143304.

[20] J.-M. Jin, *Theory and Computation of Electromagnetic Fields*. Hoboken, NJ, USA: Wiley, 2011.

[21] S. J. Orfanidis, *Electromagentic Waves and Antennas*. New Brunswick, NJ, USA: Rutgers Univ. Press, 2016.

[22] J. Nagel, "Electrostatic 2D method of moments [source code]," Metadata, 2020. https://codeocean.com/capsule/0411164/tree/v1

[23] S. M. Rao, A. W. Glisson, D. R. Wilton, and B. S. Vidula, "A simple numerical solution procedure for statics problems involving arbitrary-shaped surfaces," *IEEE Trans. Antennas Propag.*, vol. 27, no. 5, pp. 604–608, Sep. 1979, doi: 10.1109/TAP.1979.1142171.

[24] S. M. Rao, T. K. Sarkar, and R. F. Harrington, "The electrostatic field of conducting bodies in multiple dielectric media," *Adv. Electromagn.*, vol. 7, no. 3, pp. 46–55, 2018.

[25] J. Shen and O. Sterz, "A mixed Galerkin and collocation approach for treating edge and corner problems in the boundary element method," *IEEE Trans. Magn.*, vol. 34, no. 5, pp. 3296–3299, Sep. 1998, doi: 10.1109/20.717774.

Authorized licensed use limited to: UNIVERSITAT POLITECNICA DE CATALUNYA. Downloaded on December 16,2022 at 17:36:21 UTC from IEEE Xplore. Restrictions apply.